Engineering an Artificial Flavoprotein Magnetosensor.

Chris Bialas,[1,‡] Lauren E. Jarocha,[2,‡] Kevin B. Henbest,[3] Tilo M. Zollitsch,[2] Goutham Kodali,[1] Christiane R. Timmel,[3] Stuart R. Mackenzie,[2] P. Leslie Dutton,[1] Christopher C. Moser,[*,1] and P. J. Hore[*,2]

1. Johnson Research Foundation, Department of Biochemistry and Biophysics, University of Pennsylvania, Philadelphia, PA 19104, U.S.A.

2. Department of Chemistry, University of Oxford, Physical and Theoretical Chemistry Laboratory, OX1 3QZ, United Kingdom

3. Department of Chemistry, University of Oxford, Inorganic Chemistry Laboratory, OX1 3QR, United Kingdom

Supporting Information Placeholder

ABSTRACT: Migratory birds use the Earth's magnetic field as a source of navigational information. This light-dependent magnetic compass is thought to be mediated by cryptochrome proteins in the retina. Upon light activation, electron transfer between the flavin adenine dinucleotide cofactor and tryptophan residues leads to the formation of a spin-correlated radical pair, whose subsequent fate is sensitive to external magnetic fields. To learn more about the functional requirements of this complex chemical compass, we have created a family of simplified, adaptable proteins – maquettes – that contain a single tryptophan residue at different distances from a covalently bound flavin. Despite the complete absence of structural resemblance to the native cryptochrome fold or sequence, the maquettes exhibit a strong magnetic field effect that rivals those observed in the natural proteins *in vitro*. These novel maquette designs offer unprecedented flexibility to explore the basic requirements for magnetic sensing in a protein environment.

Migratory birds detect the direction of the Earth's magnetic field (25–65 μT) for the purposes of orientation and navigation on a global scale.[1] Recent evidence suggests that this light-dependent magnetic sense is mediated by cryptochromes (Cry), a class of blue-light photoreceptor proteins.[2] Mostly α-helical in structure, Crys contain a non-covalently bound flavin adenine dinucleotide (FAD) cofactor and a conserved tryptophan (Trp) triad that acts as an electron transfer chain (Fig. 1A).[3] Excitation of the FAD with blue light (< 500 nm) leads to formation of a radical pair (RP) by electron transfer from the distal Trp to the FAD along the Trp-triad.[4]

Magnetic sensitivity arises because an applied field can influence the timing and extent of interconversion of the singlet (S) and triplet (T) states of the RP.[5] Charge recombination of the RP from the T state is spin-forbidden and can only occur from the S state; therefore by altering the instantaneous probability of being S or T, an external field can change the lifetime of the RP and the yields of long-lived reaction products that could act as signaling states. Such magnetic field effects (MFEs) have been observed in Cry and a related protein (DNA photolyase), albeit in fields (1-30 mT) stronger than the geomagnetic field.[6]

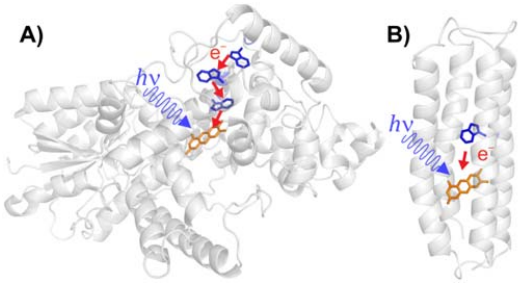

Figure 1. A) *Drosophila melanogaster* Cry. B) Representation of the W16 flavomaquette demonstrating the secondary structure and the location of the Trp residue (blue) relative to the flavin (orange). Red arrows show the photo-induced electron transfers that produce magnetically sensitive RPs.

Understanding the fundamental requirements for a magnetic compass protein[5, 7] has been hindered by the difficulty of obtaining sufficient quantities of the structurally complex natural material for spectroscopic analysis.[8] Therefore, much of what is known about the design features of RP compass sensors has come from experiments on simple model systems that, while easier to work with, are far from biologically relevant.[9]

To determine the biophysical properties required of a protein-based magnetoreceptor, we have designed a series of model proteins, known as maquettes. These are simple, robust, non-natural proteins that can be designed and adapted for specific functions in order to cut through the bewildering complexity of natural systems.[10] Maquettes have served as excellent models for understanding the functions of other proteins, including photosystem I and hemoglobin.[11] Here we demonstrate the photophysical behavior and magnetic sensitivity of a new class of flavomaquettes designed to reveal the biophysical requirements underlying the formation of a light-activated magnetically sensitive RP similar to that in Cry (Fig. S1). These are the first *de novo* proteins capable of sensing magnetic fields.

Table 1. Physical, spectroscopic, and magnetic field-sensing properties of the single-Trp series of flavomaquettes

De-sign	T_m (°C)	Φ_F[a]	τ_F (ns)[b]	Trp Fluor. max. (nm)	Flavin E_m[c] (mV vs SHE)	Trp E_m[c] (V vs SHE)	Predicted ET rate (s^{-1})[d]	MFE (%, 520-610 nm)
Con-	49.0	0.11	1.150	–	−110	–	–	0
W13	50.5	0.04	0.60	335	−137	1.10	1.49 fi 10^{10}	+16.0
W16	53.2	0.07	0.84	338	−128	1.08	6.49 fi 10^{6}	+17.5
W20	55.3	0.10	0.97	337	−130	1.06	2.83 fi 10^{3}	0

a) Quantum yield of flavin fluorescence; b) amplitude-averaged lifetime of flavin fluorescence obtained from a tri-exponential fit to TCSPC data; c) midpoint potentials; d) rate constants for forward electron transfer to the triplet state flavin predicted using the Moser–Dutton ruler.[12]

The basic flavomaquette fold is a single chain, four-α-helical bundle connected by three hydrophilic loops (Fig. 1B).[13] Each helix contains 26 amino acids and is binary patterned, with an exposed hydrophilic face and a hydrophobic face buried in the core of the α-helical bundle. For structural simplicity, the scaffold was not designed with a binding pocket for the flavin. Instead, 8-bromo-riboflavin was covalently attached to the maquette using a core cysteine at position 9 on helix 2. A core residue was replaced with Trp on helix 2 at varying distances, either one (0.56 nm, W13), two (1.12 nm, W16), or three (1.68 nm, W20) helical turns away from the site of flavin attachment (Fig. S1; distances between β-carbons of the amino acid residues of an α-helix). To avoid unwanted photochemistry, amino acids that could react with flavins were excluded (other than the unique Trp). After attachment of the flavin, the protein molecular weight was ca. 15 kDa, the exterior charge was –12 at pH 7.5, and the pI was 4.22. A flavomaquette with no Trp was developed as a control. The maquettes were expressed with high yield in *E. coli*; for details see the Supporting Information.

Circular dichroism showed that all four flavinated maquettes are highly helical in structure and thermally stable (Table 1, Fig. S4). Covalent attachment of the flavin red-shifts its absorption band from 450 nm to 475 nm (ε = 24,600 cm^{-1} mol^{-1}). Two-electron reduction of the flavin results in loss of the feature at 475 nm and formation of a weak absorption band centered at 367 nm (Fig. 2). The fluorescence of the covalently bound flavin showed no solvato-chromic shift in different maquette designs, suggesting that the cofactor experiences similar environments (Fig. S6). Additionally, the Trp fluorescence maxima are blue-shifted relative to the free amino acid, implying that the Trp residues are located well within the hydrophobic core of the maquette (Table 1). The redox potentials of the flavin and Trp indicate a favorable driving force for light-activated electron transfer in the maquette (Table 1, Fig. S8).[12] The fluorescence quantum yield is greatest for the Trp-free control and W20, and decreases with decreasing distance between the chromophore and the Trp. This is consistent with time-correlated single photon counting measurements (TCSPC, Fig. S7): the initial fluorescence intensity was comparable in all designs, but the fluorescence lifetimes decreased with decreasing flavin-Trp separation. This indicates distance-dependent quenching of the flavin fluorescence in the presence of Trp, consistent with electron transfer involving the excited singlet state of the flavin.

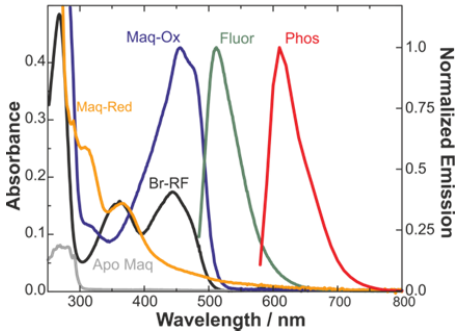

Figure 2. Absorption spectra of the apo-maquette (grey), oxidized 8-bromo-riboflavin precursor (black) and oxidized (blue) and fully reduced (orange) control flavomaquette. Normalized emission spectra of the same maquette (green - fluorescence, red - phosphorescence) are also shown.

The photochemistry of the maquettes was investigated further by nanosecond transient absorption (TA) spectroscopy. Figure 3A shows the TA spectrum of W16; that of W13 is similar (Fig. S14). There is a broad ground state bleach in the range of 400-500 nm and a strong excited state absorption at 500-650 nm consistent with the rapid formation (≪ 1 μs), by photo-induced electron transfer, of a [$F^{\bullet-}$ $TrpH^{\bullet+}$] RP,[6a] in which the $F^{\bullet-}$ radical is covalently bound to a protein at the 8-position of the flavin ring system.[14] In the control maquette and in W20, only a weak absorption band was observed at 500-800 nm with a lifetime of 17 μs (Fig. S14), assigned to the triplet excited state of the flavin.[15] Formation of the RP should be possible in W20; however, intraprotein electron tunneling rates usually drop by a factor of ca. 2300 for every 0.56 nm added by the turn of the α-helix.[12] Electron transfer in W20 (estimated in Table 1 for a donor-acceptor separation of 3 α-helical turns) is unlikely to compete with other excited state deactivation pathways, and was not observed.

The flavin radical dominates the transient spectra of W13 and W16 because the extinction coefficients of Cys-bound flavins are substantially higher than for free flavins. From a comparison with electronically similar flavins (Fig. S11), the spectrum in Fig. 3A appears to be the result of partial protonation of the flavin radical to form the neutral $FH^{\bullet}$ species around pH 7 (Fig. S12). The absorption of the Trp radicals occurs at very similar wavelengths and cannot be

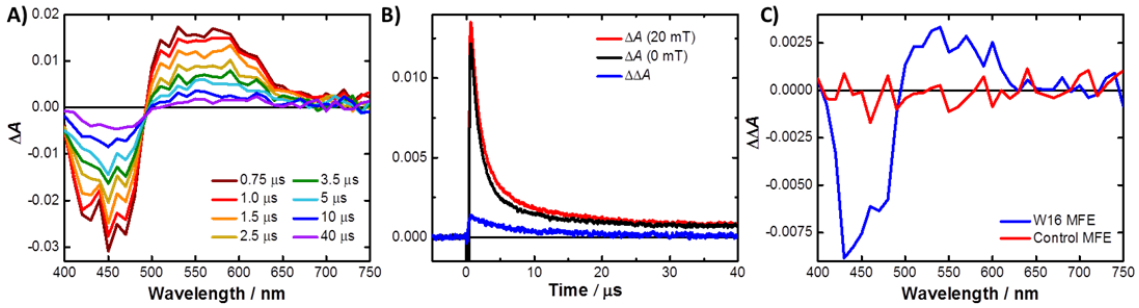

Figure 3. A) Transient absorption spectra of ca. 30 µM flavomaquette W16 at 298 K in a pH 7.4 phosphate buffer. B) Kinetic traces obtained from TA experiments at 520 nm demonstrating the difference (blue) between measurements with the field on (red) and field off (black). Data for other wavelengths may be found in Fig. S13. C) Comparison of the action spectra [$\Delta\Delta A$ = ΔA(20 mT) – ΔA(0)] showing the MFE for W16 and the control at a pump-probe delay of 1 µs.

resolved independently. However, based on the pK_a for $TrpH^{\bullet+}$ (4.3),[16] deprotonation is expected to form the neutral $Trp^{\bullet}$ radical. Both W13 and W16 have similar lifetimes for the RP (Table S3), on the order of several microseconds. This is shorter than observed in Cry proteins,[6b] but sufficiently long that MFEs can be generated and observed.

To measure the MFE, TA spectra were taken in the presence and absence of a 20 mT magnetic field at 298 K. The action spectra [$\Delta\Delta A$ = ΔA(20 mT) – ΔA(0)] of W16 (Fig. 3C) and W13 match the spectral shape of the excited state absorption between 500 and 650 nm. The negative field effect observed in the ground state bleach and positive effect in the excited state absorption are expected if the RP forms via the triplet excited state of the flavin. No MFE was observed for W20, consistent with the absence of RP signals in the TA spectrum. Likewise, the control maquette showed no measurable MFE, further supporting the view that there is no magnetically sensitive intra- or intermolecular chemistry in the absence of a Trp residue.

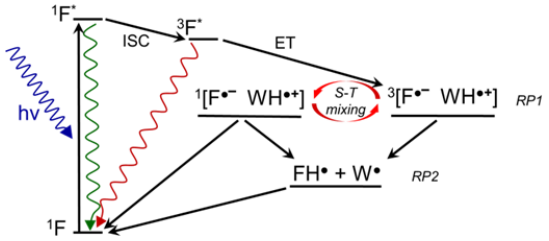

Scheme 1: Proposed photochemistry of the flavomaquettes leading to the observed triplet-born MFE.

The spectra and MFEs observed for these flavomaquettes are consistent with Scheme 1. After excitation, a fraction of the excited flavin ($^1F^*$) undergoes intersystem crossing (ISC) to form the excited triplet state ($^3F^*$). The primary spin-correlated RP, denoted RP1, is formed as a triplet by electron transfer from the Trp to the excited triplet flavin. RP1 can undergo S–T interconversion induced by electron-nuclear hyperfine interactions. In the presence of a strong field, the Zeeman interaction removes the degeneracy of the triplet RP energy levels, reduces the efficiency of spin-mixing, and leads to a MFE. Protonation of the flavin radical or deprotonation of the Trp radical creates the secondary radical pair, RP2, observed in our TA measurements, which eventually returns to the ground state.

The fractional MFEs [(ΔA(20 mT) – ΔA(0))/ΔA(0)] for W13 and W16 are comparable, but the absolute magnitude [ΔA(20 mT) – ΔA(0)] is smaller for W13 (Fig. S14). This probably results from competition between singlet- and triplet-born RP formation in W13, where the smaller flavin-Trp distance leads to a faster forward electron transfer that competes with ISC. Rapid formation of a singlet-born RP is consistent with the increased quenching and shorter fluorescence lifetimes observed by TCSPC. However, the positive MFE indicates that formation of the RP must also occur via the triplet route. Singlet photochemistry is not observed on the microsecond timescale because charge recombination rapidly returns the singlet RPs to the ground state. Charge recombination is initially spin-forbidden for triplet-born RPs which, therefore, have a longer lifetime and contribute more strongly to the MFE.

Triplet-dominated photochemistry in the maquettes is in direct contrast to Cry, which forms a RP from the singlet excited state. This is not surprising: ISC is certainly faster in flavomaquettes than in Cry because of increased spin-orbit coupling due to the Cys sulfur atom attached directly to the flavin ring system. Additionally, for W16 and W20, electron transfer rates are probably slower than those observed in Cry. However, the difference in the spin state of the excited flavin leading to the RP does not affect the ability of the maquettes to serve as a model for elucidating the principles of efficient protein-based sensing of magnetic fields. In fact, triplet-born photochemistry is arguably advantageous for such a simple model system. Given the short distances and large driving force in W13 and W16, the singlet RP is expected to undergo rapid charge recombination. The triplet spin state stabilizes the RP in the maquettes, while natural proteins must rely on physical separation of the charges using an electron transfer chain or conformational changes to achieve the same end. The extension of the RP lifetime in the maquettes due to its triplet spin state allows the observation of a room temperature (298 K) MFE of ~16% at 20 mT on a microsecond timescale, comparable in magnitude to that of *Arabidopsis thaliana* Cry-1 or *E. coli* photolyase (12-17% at 28 mT).[6b] Such large MFEs in natural systems are only observed at reduced temperatures (278 K and below) and in the presence of large amounts of glycerol.

This work represents the first report of an artificial protein-based magnetic sensor. The ease of production and modification of maquettes make them an ideal model system for investigating the basic requirements of protein-based magnetoreception. Developing a thorough understanding of these principles would be an important step toward the elu-

cidation of the biophysical mechanism of the avian magnetic compass. Future work will focus on applying cavity-enhanced and transient absorption spectroscopies[17] to these novel proteins to fully resolve the kinetic and spectra properties of the RP. These early findings are being used to design maquettes that contain two and three Trp residues, with the intention of creating a light-activated electron transport chain akin to that found in photolyases and cryptochromes.

ASSOCIATED CONTENT

Supporting Information

Supporting information includes detailed materials and methods, HPLC, mass spectroscopy, peptide sequence, circular dichroism, spectro-electrochemistry, fluorescence, TCSPC, and transient absorption data including pH dependence, kinetic traces, and spectra and MFEs for the control, W13, and W20. This material is available free of charge via the Internet at http://pubs.acs.org.

AUTHOR INFORMATION

Corresponding Authors

* peter.hore@chem.ox.ac.uk
* moserc@mail.med.upenn.edu

Author Contributions

‡These authors contributed equally.

Notes

The authors declare no competing financial interests.

ACKNOWLEDGMENT

We are grateful to the following for financial support: the European Research Council (under the European Union's 7th Framework Programme, FP7/2007-20013/ERC Grant Agreement No 340451 to PJH), and the Air Force Office of Scientific Research (Air Force Materiel Command, USAF Award No. FA9550-14-1-0095 to PJH, CRT, and SRM). C.B. is grateful to NIH for a graduate fellowship (T32 GM008275 - Structural Biology & Molecular Biophysics Training Program). We thank G. A. Logsdon for help with molecular biology, S. A. Vinogradov for the use of his phosphorimeter and useful discussion, and T. Troxler of the Ultrafast Optical Processes Laboratory at the University of Pennsylvania (NIH Resource Grant P41-104605) for use of his TCSPC equipment.

REFERENCES

1. Mouritsen, H., *Magnetoreception in Birds and Its Use for Long-Distance Migration*, in *Sturkie's Avian Physiology* (*Sixth Edition*), Scanes, C. G. (Ed.); Elsevier: New York, 2015; pp 113-133.

2. (a) Liedvogel, M.; Mouritsen, H., *J. R. Soc., Interface* **2010,** *7*, S147-S162; (b) Hore, P. J.; Mouritsen, H., *Annu. Rev. Biophys.* **2016,** *45*, 299-344.

3. Chaves, I.; Pokorny, R.; Byrdin, M.; Hoang, N.; Ritz, T.; Brettel, K.; Essen, L.-O.; van der Horst, G. T. J.; Batschauer, A.; Ahmad, M., *Annu. Rev. Plant Biol.* **2011,** *62*, 335-364.

4. Immeln, D.; Weigel, A.; Kottke, T.; Lustres, J. L. P., *J. Am. Chem. Soc.* **2012,** *134*, 12536-12546.

5.Rodgers, C. T.; Hore, P. J., *Proc. Natl. Acad. Sci. U. S. A.* **2009,** *106*, 353-360.

6. (a) Henbest, K. B.; Maeda, K.; Hore, P. J.; Joshi, M.; Bacher, A.; Bittl, R.; Weber, S.; Timmel, C. R.; Schleicher, E., *Proc. Natl. Acad. Sci. U. S. A.* **2008,** *105*, 14395-14399; (b) Maeda, K.; Robinson, A. J.; Henbest, K. B.; Hogben, H. J.; Biskup, T.; Ahmad, M.; Schleicher, E.; Weber, S.; Timmel, C. R.; Hore, P. J., *Proc. Natl. Acad. Sci. U. S. A.* **2012,** *109*, 4774-4779.

7. Brocklehurst, B., *Chem. Soc. Rev.* **2002,** *31*, 301-311.

8.Evans, E. W.; Dodson, C. A.; Maeda, K.; Biskup, T.; Wedge, C. J.; Timmel, C. R., *Interface Focus* **2013,** *3*, 20130037

9. Maeda, K.; Henbest, K. B.; Cintolesi, F.; Kuprov, I.; Rodgers, C. T.; Liddell, P. A.; Gust, D.; Timmel, C. R.; Hore, P. J., *Nature* **2008,** *453*, 387-390.

10. Moser, C. C.; Sheehan, M. M.; Ennist, N. M.; Kodali, G.; Bialas, C.; Englander, M. T.; Discher, B. M.; Dutton, P. L., *Methods Enzymol.* **2016**, *580*, 365-388.

11.(a) Lichtenstein, B. R.; Bialas, C.; Cerda, J. F.; Fry, B. A.; Dutton, P. L.; Moser, C. C., *Angew. Chem., Int. Ed.* **2015,** *54*, 13626-13629; (b) Goparaju, G.; Fry, B. A.; Chobot, S. E.; Wiedman, G.; Moser, C. C.; Dutton, P. L.; Discher, B. M., *Biochim. Biophys. Acta, Bioenerg.* **2016,** *1857*, 503-512; (c) Koder, R. L.; Anderson, J. L. R.; Solomon, L. A.; Reddy, K. S.; Moser, C. C.; Dutton, P. L., *Nature* **2009,** *458*, 305-309.

12. Page, C. C.; Moser, C. C.; Chen, X.; Dutton, P. L., *Nature* **1999,** *402*, 47-52.

13.Farid, T. A.; Kodali, G.; Solomon, L. A.; Lichtenstein, B. R.; Sheehan, M. M.; Fry, B. A.; Bialas, C.; Ennist, N. M.; Siedlecki, J. A.; Zhao, Z.; Stetz, M. A.; Valentine, K. G.; Anderson, J. L. R.; Wand, A. J.; Discher, B. M.; Moser, C. C.; Dutton, P. L., *Nat Chem Biol* **2013,** *9*, 826-833.

14.(a) Raibekas, A. A.; Fukui, K.; Massey, V., *Proc. Natl. Acad. Sci. U. S. A.* **2000,** *97*, 3089-3093.

15.Mansurova, M.; Simon, J.; Salzmann, S.; Marian, C. M.; Gärtner, W., *ChemBioChem* **2013,** *14*, 645-654.

16.Posener, M. L.; Adams, G. E.; Wardman, P.; Cundall, R. B., *J. Chem. Soc., Faraday Trans. 1* **1976,** *72*, 2231-2239.

17.(a) Neil, S. R. T.; Li, J.; Sheppard, D. M. W.; Storey, J.; Maeda, K.; Henbest, K. B.; Hore, P. J.; Timmel, C. R.; Mackenzie, S. R., *J. Phys. Chem. B* **2014,** *118*, 4177-4184; (b) Maeda, K.; Neil, S. R. T.; Henbest, K. B.; Weber, S.; Schleicher, E.; Hore, P. J.; Mackenzie, S. R.; Timmel, C. R., *J. Am. Chem. Soc.* **2011,** *133*, 17807-17815.

Supplementary Information

Engineering an Artificial Flavoprotein Magnetosensor.

Chris Bialas,[1‡] Lauren E. Jarocha,[2‡] Kevin B. Henbest,[3] Tilo M. Zollitsch,[2] Goutham Kodali,[1] Christiane R. Timmel,[3] Stuart R. Mackenzie,[2] P. Leslie Dutton,[1] Christopher C. Moser,*[,1] and P. J. Hore*[,2]

1. Johnson Research Foundation, Department of Biochemistry and Biophysics, University of Pennsylvania, Philadelphia, PA 19104, U.S.A.

2. Department of Chemistry, University of Oxford, Physical and Theoretical Chemistry Laboratory, OX1 3QZ, United Kingdom

3. Department of Chemistry, University of Oxford, Inorganic Chemistry Laboratory, OX1 3QR, United Kingdom

Table of Contents

Materials and Methods

Unless otherwise noted, all of the reagents were commercially available from Fischer Scientific or Sigma Aldrich.

Protein expression and purification

The original design first described in Farid *et al.* (2013) was constructed as a synthetic gene from DNA2.0 in a PJ414 vector.[1] All designs were generated using PCR mutagenesis from this parent vector. Mutagenesis was carried out using AccuPrime™ Pfx SuperMix (Invitrogen). A volume of 22.5 µL of AccuPrime™ Pfx SuperMix was combined with 1 µL of solution containing 100 ng of parent DNA, 0.5 µL of a 100 µM solution of each primer and 2.7 µL of MasterAmp PCR Enhancer. The sample was cycled on an Eppendorf Master Cycler Pro (model 6321) using the following procedure: initial denaturation at 95 °C for 5 minutes, followed by repeating a cycle of denaturation at 95 °C for 15 seconds, annealing at 65 °C for 30 seconds, and extension at 68 °C for 5 minutes for a total of 18 times. A final extension was done at 68 °C for 5 minutes and ended with a hold at 4 °C. Samples were then digested with 0.5 µL of Dpn-1 (New England Biolabs) for 1 hour at 37 °C. A volume of 1 µL of this DNA was transformed into DH5 α cells (Genechoice Genesee Scientific) and grown overnight on an LB agar ampicillin plate (75 mg/ml) at 37 °C. The following day, four single colonies were picked and outgrown in LB media with ampicillin and their DNA was extracted using a Miniprep Kit (Qiagen). The sequence was verified at the University of Pennsylvania DNA sequencing Core Facility using a T7 promoter primer.

All constructs were designed with a six-histidine tag separated by a TEV cleavage site (Scheme S1). All were expressed in *E. coli* BL21 (DE3) cells (Genechoice Genesee Scientific). Two liter cultures of TB media where grown to OD_{600} 0.7-0.8 at 37 °C, followed by a 5-hour induction with 1 mM IPTG. The cells were harvested by centrifugation (10000 RPM, 5 minutes) and stored at 20 °C until use. Cells were thawed and suspended in Ni Wash buffer (20 mM NaH_2PO_4, 0.5 M NaCl, 10 mM imidazole, pH 8.0) with 1% OTG, then homogenized and lysed by sonication in a bath sonicator. The lysate was centrifuged (25,000*g*, 35 min) and the supernatant applied to a NiNTA superflow resin (Qiagen) on an Akta Fast protein liquid chromatography (FPLC) system. The fusion protein was eluted using Ni Elution buffer (20 mM NaH_2PO_4, 0.5 M NaCl, 250 mM imidazole, pH 8.0), and cleaved by recombinant tobacco etch virus N1a(TEV) protease overnight at room temperature in Ni Elution buffer supplemented with 1 mM TCEP (reductant) and 0.5 mM EDTA. The sample was dialyzed into Ni Wash buffer, and applied to the NiNTA column with the flow through and wash collected. The sample was then concentrated to about 15 mL using a stirred cell (Amicon model 8050) equipped with a 10,000 MWC filter. The sample was flash frozen in liquid nitrogen and stored at −20 °C until use.

Flavination of the maquettes

The protein was flavinated using an optimized version of a protocol first described in Farid *et al*. *(*2013).[1] A typical 5 mL reaction contained concentrated maquette (a few hundred millimolar, in Ni Wash), a 3-5 molar excess of 8-bromoriboflavin (in DMF, final DMF concentration not to exceed 20%), and TCEP at a final concentration of 1.25 mM. The pH of the solution was adjusted to 9.0 with NaOH, and stirred overnight at 50 °C while protected from light. The sample was purified on a Waters reverse-phase HPLC (C18 column Gracie, H_2O + 0.1% TFA aqueous phase and acetonitrile +

0.1% TFA organic phase), flash frozen in liquid nitrogen and lyophilized (Figure S1). Flavination was verified by the presence of a 475 nm band on the HPLC detector as well as by ESI, matrix assisted laser desorption ionization mass spectrometry.

Matrix assisted laser desorption ionization mass spectrometry

Samples were either taken directly from the HPLC or, if they had been lyophilized, dissolved in 66% acetonitrile, 44% water + 0.1% TFA. A sample volume of 1 µL was mixed with 1 µL of saturated matrix solution (sinapinic acid in TFA) and spotted on a sample target. The target was then dried under vacuum and measurements taken in linear flight mode (Figure S2).

Spectroscopic characterization

The sample was dissolved in redox buffer (20 mM KH_2PO_4, 100 mM KCl, pH 7.4). All measurements were in this buffer unless otherwise stated.

UV-visible spectra (Figure 2, Figure S4) were collected in a quartz cuvette (1 mL, 1 cm path) with a Varian Cary-50 spectrophotometer at room temperature. The presence of a band at 475 nm indicated incorporation of the flavin under normal (oxidizing) conditions. UV-visible spectra used to monitor photodegradation and concentration prior to transient absorption experiments were collected with a Varian Cary-60 spectrometer, using a small volume quartz cuvette (1 cm path length, 200 µL volume) at room temperature.

Secondary structure was monitored by CD spectroscopy (Aviv Model 410) with a quartz cuvette (400 µL, 1 mm path) from 200 nm to 300 nm at 25 °C (Figure S3A). The thermal stability was determined by monitoring the ellipticity at 222 nm every 2 °C from 2 °C to 98 °C (Figure S3B). The melting temperatures were calculated using a single term Boltzmann fit. Typical concentration was 20-30 µM.

Steady state fluorescence data (Table 1 and Figure S5) where analysed in a quartz fluorescence cuvette (1 ml, 1 cm path) on a Horiba Fluorolog 2 spectrophotometer at 20 °C. All spectra where corrected for fluctuations in lamp intensity. Typical concentrations were 3-5 µM (OD_{475} 0.05-0.1). Quantum yield measurements were made by integrating the area under the curve of the steady state spectrum relative a riboflavin standard (Φ = 0.267)[2] and correcting for concentration and extinction.

Fluorescence lifetimes where determined using a time-correlated single photon counting (TCSPC) spectrometer at the Ultrafast Optical Processes Laboratory at the University of Pennsylvania. Samples were prepared in redox buffer at approximately 5 µm (OD_{475} = 0.1) at room temperature in a quartz cuvette (1 mL, 1 cm path). A 482 nm picosecond diode laser (PicoQuant GmbH; Berlin, Germany) was used as an excitation source. Emission was recorded at 512 nm on a Becker-Hickl TCSPC board and analysed with FluoFit software (Picoquant). The best fit was a triple exponential (Figure S6). All spectra where corrected for fluctuations in lamp intensity.

The steady state phosphorescence spectrum (Figure 2) was recorded on an Edinburgh Instruments FS 920 Fluorimeter equipped with a liquid nitrogen dewar. A sample volume of 200 µM was flash frozen in a glass tube and spectra taken at liquid nitrogen temperatures.

Electrochemical characterization

Redox titrations (Table 1, Figure S7A) were performed to determine the redox potential fo the flavin using a spectroelectrochemical system. A typical sample contained 10-30 μM protein and the following redox mediators: duroquinone (10 μM), pyocyanin (10 μM), 2-hydroxy-1,4-naphthoquinone (10 μM), phenazine (10 μM), anthraquinone-2-sulfonate (20 μM), benzyl viologen (10 μM), and methyl viologen (10 μM). The potential of the solution was modulated from 0 mV to –500 mV vs. S.H.E. using a CH Instruments model 600C electrochemical analyser equipped with a Pine Instruments gold honeycomb electrode. The electrode was coated to prevent protein build-up by soaking in 2 mM cystamine for 45 minutes. The oxidation state of the system was monitored spectroscopically using an Ocean Optics DH-2000-BAL light source and a fiber-optic-guided USB 4000 diode array detector. The change from oxidized to reduced was monitored by the depletion in absorbance of the S1 band region of the flavin (475 nm). The data were then fitted to a Nernst equation (Eq. 1), where E_{cell} is the redox potential of the spectrochemical cell, E_m is the redox potential of the flavin, n is the number of electrons transferred and [ox, red] is the concentration of oxidized or reduced species present at a particular E_{cell}.

$$E_{\text{cell}} = E_{\text{m}} + \left(\frac{0.059}{n}\right)\log\left(\frac{[\text{ox}]}{[\text{red}]}\right) \quad (1)$$

At the redox potential (E_m), we saw no evidence of any semiquinone absorption, indicating an unstable flavin semiquinone and n=2 was used for the fit.

Square wave voltammetry was used to record the midpoint potential of the TrpH/$TrpH^{\bullet+}$ redox couple (Table 1, Figure S7B). A gold electrode was sonicated in an Alconox solution for 5 minutes in a bath sonicator followed by polishing with alumina slurry (20 nm) for 1 minute in a figure of eight motion. The electrode was then rinsed, and sonicated for 5 minutes in distilled water. Electrochemical cleaning was performed in 0.5 mM sulfuric acid from −0.375 to 1.8 V for 50 cycles using a CH Instruments model 600C electrochemical analyser. The electrode was again rinsed with distilled water, then DMSO, and coupled to dithiobis(succinimidyl propionate) (DSP, Lomant's Reagent) in DMSO (4 mg/mL) for 30 minutes. The electrode was dipped into a concentrated protein solution in redox buffer (100 μL) for 2 hours to couple it to the DSP-bound electrode. The electrode was placed into a cell containing redox buffer and equipped with a Pt counter electrode and an Ag/AgCl reference electrode. The potential was swept from 0.7 V to 1.2 V vs. S.H.E. with a frequency of 300 Hz and a 25 mV step size. Each data point was the average of five separate scans. The background current due to the gold electrode was subtracted out in post-processing.

Electron transfer rate calculations

Predicted electron transfer rates were calculated using the Moser-Dutton Ruler (see below, Eq. (1)), an empirical expression that relates the rate of electron transfer in proteins to the edge-to-edge distance between donor and acceptor (*R*, in Angstroms), the driving force of the transfer (ΔG) and the reorganization energy (λ). The distance in the flavomaquettes is a rough estimate determined using the distance between the β carbon of the ligating cysteine and the Trp. Each helical turn was approximately 5.6 Å. It should be noted that these distances are obtained from a

model of general protein structure and do not take into account any conformational flexibility that may be present for the relevant cofactors. The driving force was calculated as the difference between the excited state of the flavin singlet or triplet (calculated from the S_0 or T_0 emission wavelength, respectively), and the redox potential of the reduced flavin and oxidized Trp radical (determined in this work). The reorganization energy is difficult to determine experimentally and a medium-to-large value was estimated for small polar maquettes. Therefore, these rates are strictly used as a rough estimate for the relative timescales and behaviour expected in the flavomaquettes. For a more complete discussion of reorganization energy and estimation in the Moser-Dutton Ruler see Moser *et al*. (2010).[3]

$$\log K_{\mathrm{ET}} = 13 - 0.6\left(R - 3.6\right) - 3.1\left(\Delta G + \lambda\right)^2 / \lambda \qquad (2)$$

General ΔG calculations

ΔG = (Redox Potential F/$F^{\bullet -}$ + Photon Energy) – (Redox Potential TrpH/ $TrpH^{\bullet +}$)

Specific ΔG values

ΔG(Singlet Electron Transfer) = -1.21 V

ΔG(Singlet Charge Recombination) = -1.2 V

ΔG(Triplet Electron Transfer) = -0.81 V

ΔG(Triplet Charge Recombination) = -1.2 V

Reorganization Energy

λ = 1.2 V

Table S1. Electron transfer and charge recombination rates from the flavin singlet excited state

Singlet Electron Transfer					
		Forward Electron Transfer		Charge Recombination	
Design	**Distance (Å)**	**log(k_{ET}/s^{-1})**	**k_{ET}/s^{-1}**	**log(k_{CR}/s^{-1})**	**k_{CR}/s^{-1}**
W 13	5.6	11.21	1.61×10^{11}	11.18	1.51×10^{11}
W 16	11.2	7.85	7.01×10^{7}	7.82	6.61×10^{7}
W 20	16.8	4.49	3.06×10^{4}	4.46	2.88×10^{4}

Table S2. Electron transfer and charge recombination rates from the flavin triplet excited state

Triplet Electron Transfer					
		Forward Electron Transfer		Charge Recombination	
Design	**Distance (Å)**	**log(k_{ET}/s^{-1})**	**k_{ET}/s^{-1}**	**log(k_{CR}/s^{-1})**	**k_{CR}/s^{-1}**
W 13	5.6	10.17	1.49×10^{10}	11.18	1.51×10^{11}
W 16	11.2	6.81	6.49×10^{6}	7.82	6.61×10^{7}
W 20	16.8	3.45	2.83×10^{3}	4.46	2.88×10^{4}

It is important to note that charge recombination rates calculated for the triplet electron transfer *only take into account the energetic considerations* for the charge recombination and neglect the fact that recombination is *spin forbidden for triplet radical pairs*.

Transient absorption and magnetic field effect measurements

The transient absorption spectrometer used to characterize maquette photochemistry and measure the magnetic field effect has been described elsewhere.[4] Briefly, 250 µL of sample is placed in a quartz cuvette (Hellma 104.002F QS, 10 mm path length, internal dimensions 2 × 10 × 45 mm) in the center of a cryostat (Oxford Instruments, Optistat CF) with the temperature controlled at 25.0 ± 0.1 K. Magnetic field pulses of approximately 4 ms duration were synchronized with the laser flash and generated using home-built Helmholtz coils. The maximum field at the position of the sample is 20 mT. Data were collected by alternating measurements with the magnetic field on and off.

Maquettes were prepared in redox buffer to a concentration of approximately 30 µM. Dissolution of the maquette resulted in a drop of the solution pH to a value of between 6.8 and 7.0 when starting with a phosphate solution at pH 7.4. Samples were centrifuged to remove any aggregates for 15 minutes at 9000 RPM and 4 °C and then measured by UV-visible spectroscopy.

Radical pairs were generated by flash photolysis using a Sirah Cobra dye laser pumped by a Continuum Surelite I Nd:YAG laser. Excitation was 5-7 mJ at 450 nm using Coumarin 460 as the dye in analytical grade methanol (Fischer Scientific). The repetition rate for data collection was 1 Hz for W13 and W16. This repetition rate was reduced for W20 and the control, where a 1-2 minute delay between shots was necessary to avoid complications caused by photoproduct formation (Figure S8, S9). Probe light was provided by a 1000 W xenon arc lamp (Oriel) passed through water and long pass filters to minimize exposure of the sample to unwanted wavelengths. The probe beam was set perpendicular to the pump excitation. Both pump and probe beams were controlled by mechanical shutters to reduce photodegradation of the samples. The transient absorption signal was detected using a monochromater (Oriel 77250) and photomultiplier tube (Hamamatsu R928) connected to an oscilloscope (LeCroy Waverunner LT342L). Data were transferred to a computer and analysed using Igor Pro (Wavemetrics Inc.) software.

Photoproduct characterization

During the course of spectroscopic characterization, an absorption band at 400 nm began to appear concurrently with the disappearance of the 475 nm feature. We attributed this to photodamage of the flavin. To identify this product, a 10 μM sample of flavin in redox buffer was deoxygenated by exchanging the atmosphere with high purity argon (Airgas) passed through a Vd scrubbing system for 30 minutes under stirring and illuminated for 1 hour. The sample was then studied using mass spectrometry and fluorescence spectroscopy (Figures S8, S9). From the data it was concluded that the major degradation product was maquettes-coupled lumichrome, consistent with known photodegradation pathways of free flavins in solution.[5]

Control

MHHHHHHGGDGGTENLYFQG

1. EIQKQFEDALQKFEEALNQFEDLKQL GGSGSGSGG
2. EIQKQFEDCLQKFEEALNQFEDLKQL GGSGSGSGG
3. EIQKQFEDALQKFEEALNQFEDLKQL GGSGSGSGG
4. EIQKQFEDALQKFEEALNQFEDLKQL

W16

1. GEIQKQFEDALQKFEEALNQFEDLKQL GGSGSGSGG
2. EIQKQFEDCLQKFEEWLNQFEDLKQL GGSGSGSGG
3. EIQKQFEDALQKFEEALNQFEDLKQL GGSGSGSGG
4. EIQKQFEDALQKFEEALNQFEDLKQL

W13

1. GEIQKQFEDALQKFEEALNQFEDLKQL GGSGSGSGG
2. EIQKQFEDCLQKWEEALNQFEDLKQL GGSGSGSGG
3. EIQKQFEDALQKFEEALNQFEDLKQL GGSGSGSGG
4. EIQKQFEDALQKFEEALNQFEDLKQL

W20

1. GEIQKQFEDALQKFEEALNQFEDLKQL GGSGSGSGG
2. EIQKQFEDCLQKFEEALNQWEDLKQL GGSGSGSGG
3. EIQKQFEDALQKFEEALNQFEDLKQL GGSGSGSGG
4. EIQKQFEDALQKFEEALNQFEDLKQL

Scheme S1. The amino acid sequences of all of the designs. The control maquette is shown with its upstream tag sequence: the start methionine (red), six-histidine tag (green), linker (light blue) and TEV site (purple) are highlighted in color. The helices and loops, which consist only of Gly and Ser residues, are shown on separate lines from the N to C terminus, and numbered in the same order they appear in the sequence. The flavin-binding cysteine (helix 2, position 9) is shown in orange and the tryptophan in blue on helix 2.

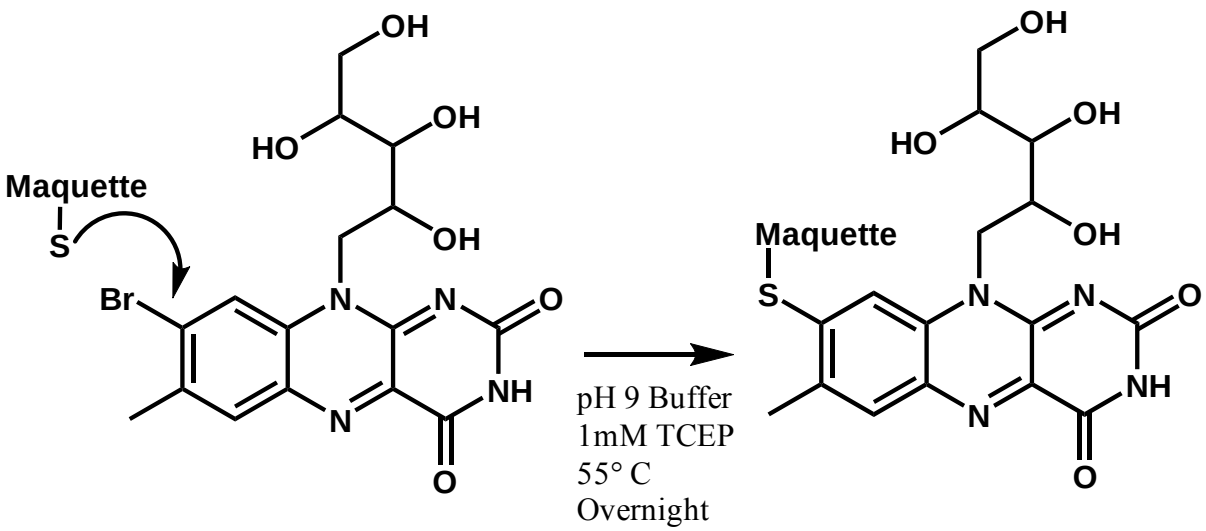

Scheme S2. The covalent attachment of 8-Br-riboflavin to a cysteine in the maquette. The reaction is performed in a high-pH buffer to ensure cysteine deprotonation and protected from light. TCEP is included to reduce inter-maquette disulphide bonds. Thiol based reductants are avoided to prevent side reactions with the flavin.

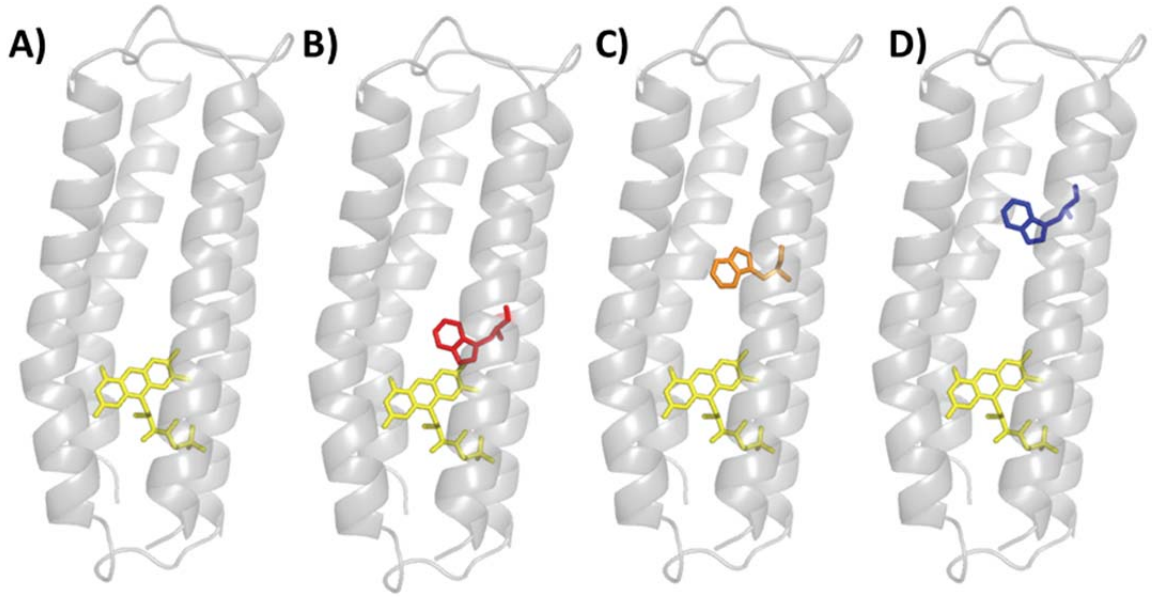

Figure S1. A representation of the four maquette designs used in these studies: A) the flavin-only control, B) W13 with the Trp one helical turn away from the flavin, C) W16 with the Trp two helical turns away from the flavin, and D) W20 with the Trp three helical turns away from the flavin.

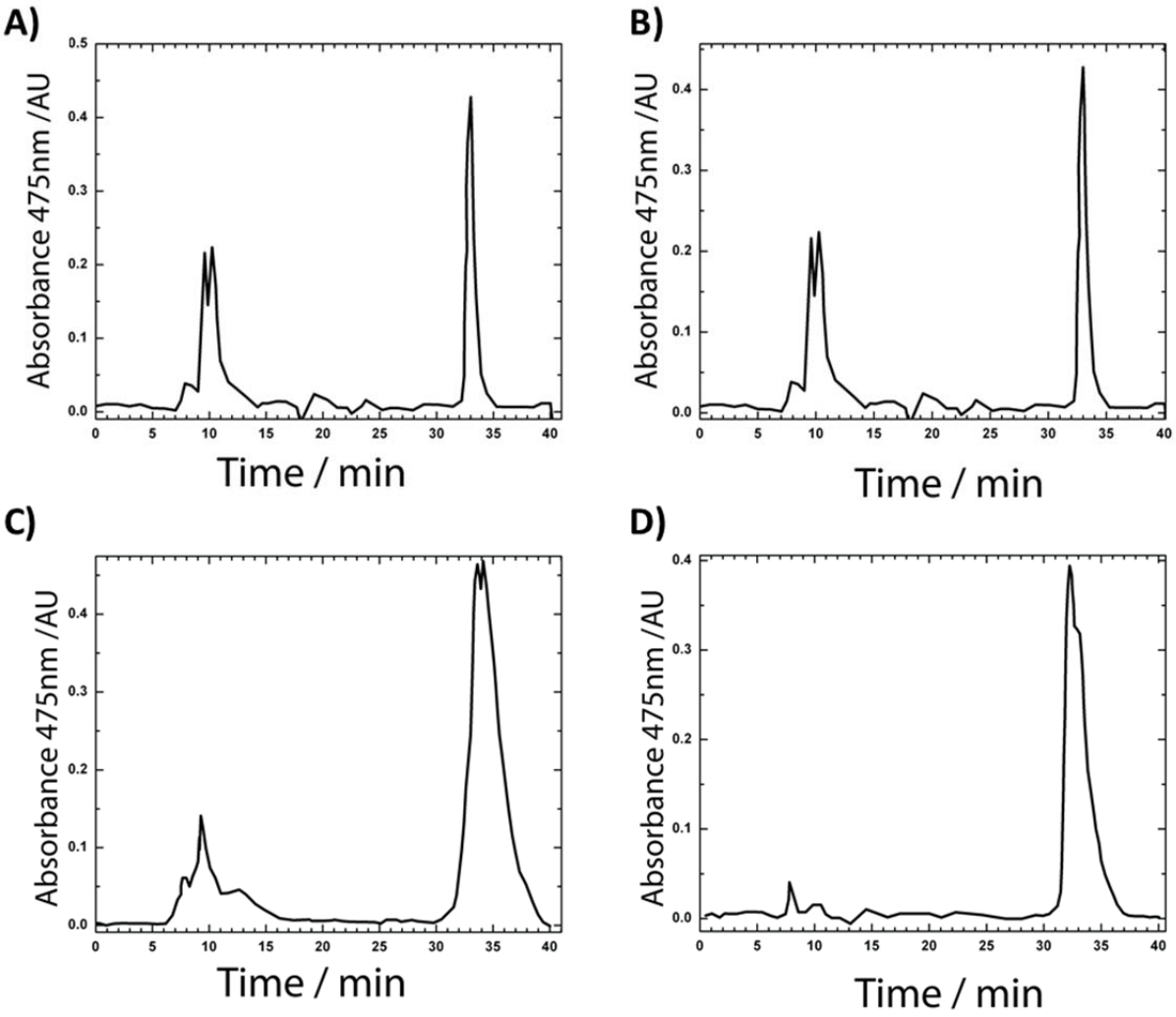

Figure S2. Reverse-phase HPLC traces of flavomaquettes: control (A), W13 (B), W16 (C) and W20 (D) taken at 475 nm. The sample was purified on a Waters reverse-phase HPLC (C18 column Gracie, H_2O + 0.1 % TFA aqueous phase and acetonitrile + 0.1% TFA organic phase). A 20-70% linear gradient of acetonitrile was used over 50 minutes to elute the protein at approximately 31 minutes. Injection peaks are present at approximately 10 minutes.

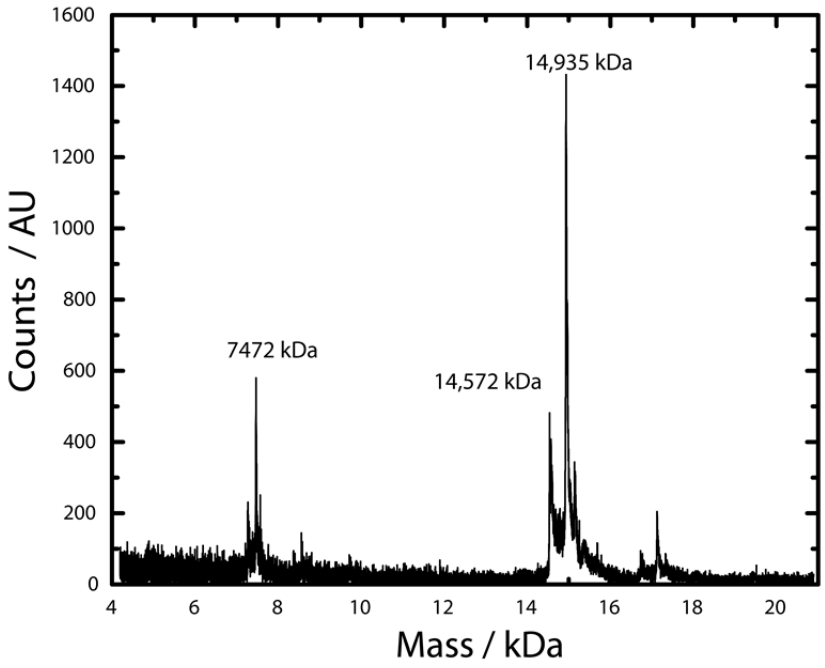

Figure S3. MALDI-TOF mass spectra of the control flavomaquette. The apo-protein appears at 14572 *m*/*z*, while the flavinated protein appears at 14935 *m*/*z*, 363 mass units higher, confirming the covalent attachment of the flavin.

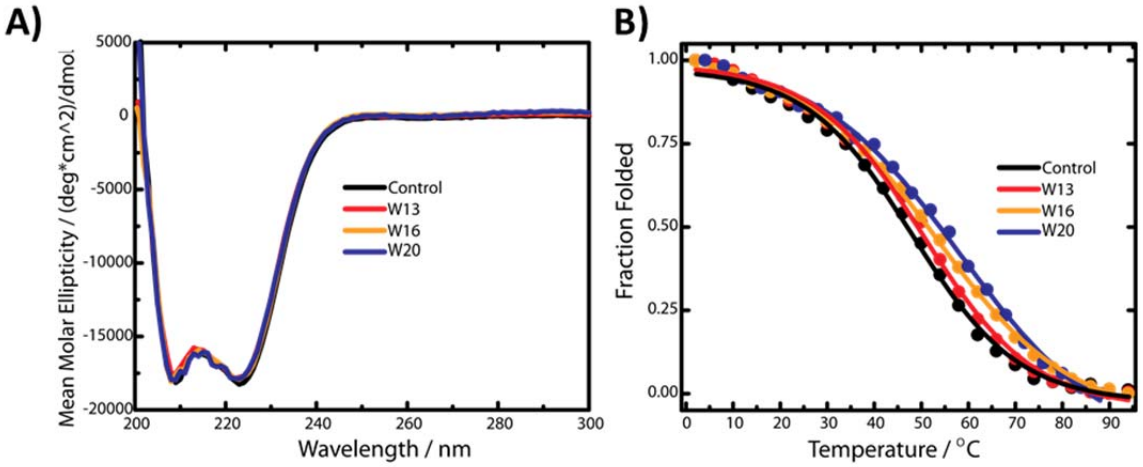

Figure S4. A) CD traces of the flavomaquettes with Trp residues at position W13, W16, and W20. The relative intensities at 208 nm and 222 nm suggest the maquette protein structure consists primarily of an α-helical bundle. B) Thermal stability curves of various flavomaquette designs. The T_m for each maquette is determined by monitoring the loss of helicity at 222 nm and fitting to a single Boltzmann distribution; control (black) 49 °C, W13 (red) 50.5 °C, W16 (orange) 53.2 °C and W20 (blue) 58.3 °C.

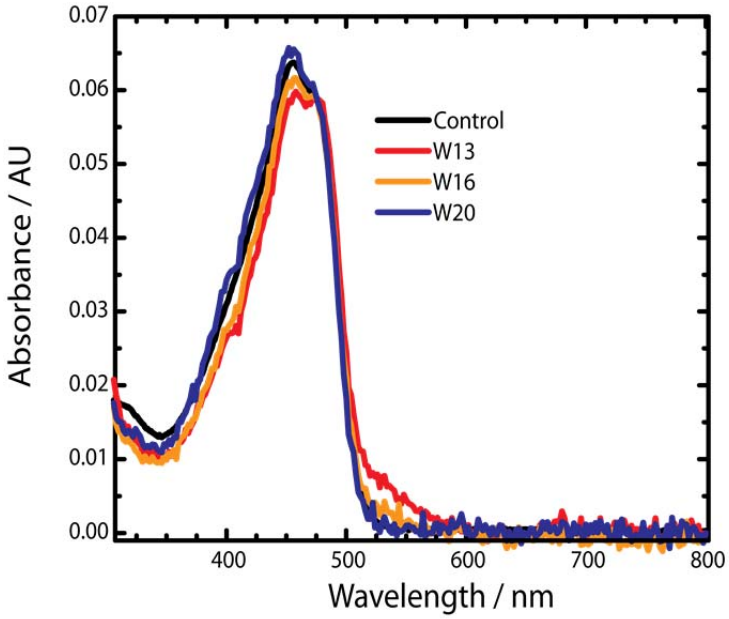

Figure S5. A comparison of the UV-visible spectra of the flavomaquette designs. The shoulder around 525 nm suggests a charge transfer band that increases as the flavin and Trp distance decreases.

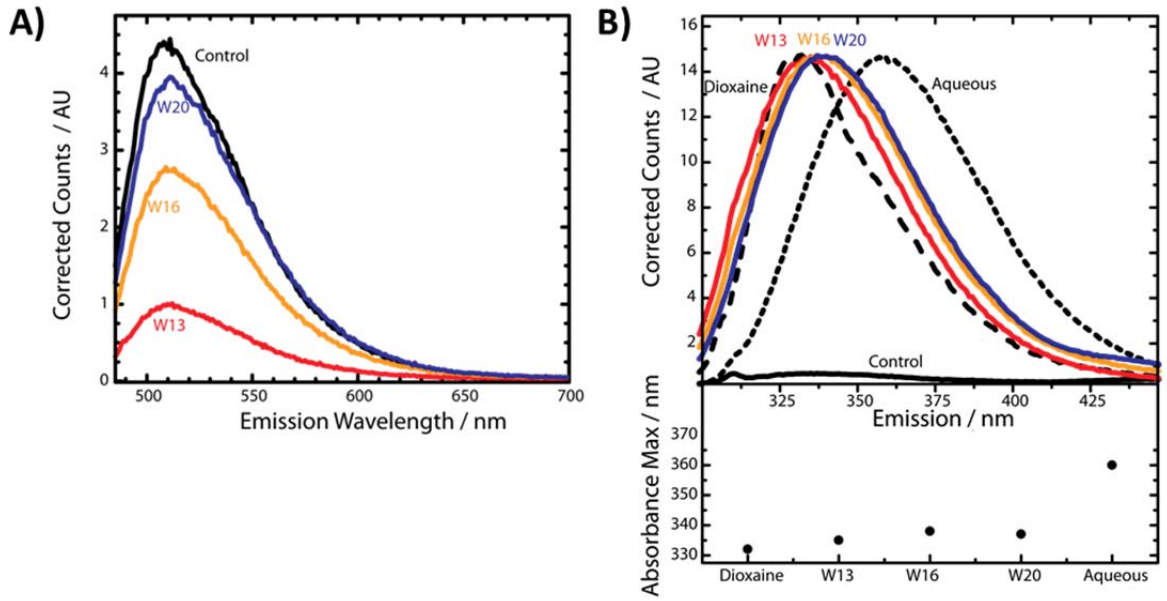

Figure S6. A) Steady state fluorescence of the flavin incorporated in the maquettes with varying flavin-Trp distances. B) A comparison of the normalized Trp fluorescence of the flavomaquette series. Free Trp in dioxane and an aqueous buffer are used as solvatochromic standards. The maximum of the Trp fluorescence in all the maquettes is blue-shifted relative to the aqueous standard, consistent with the Trp being located in the hydrophobic interior of the maquette α-helical bundle.

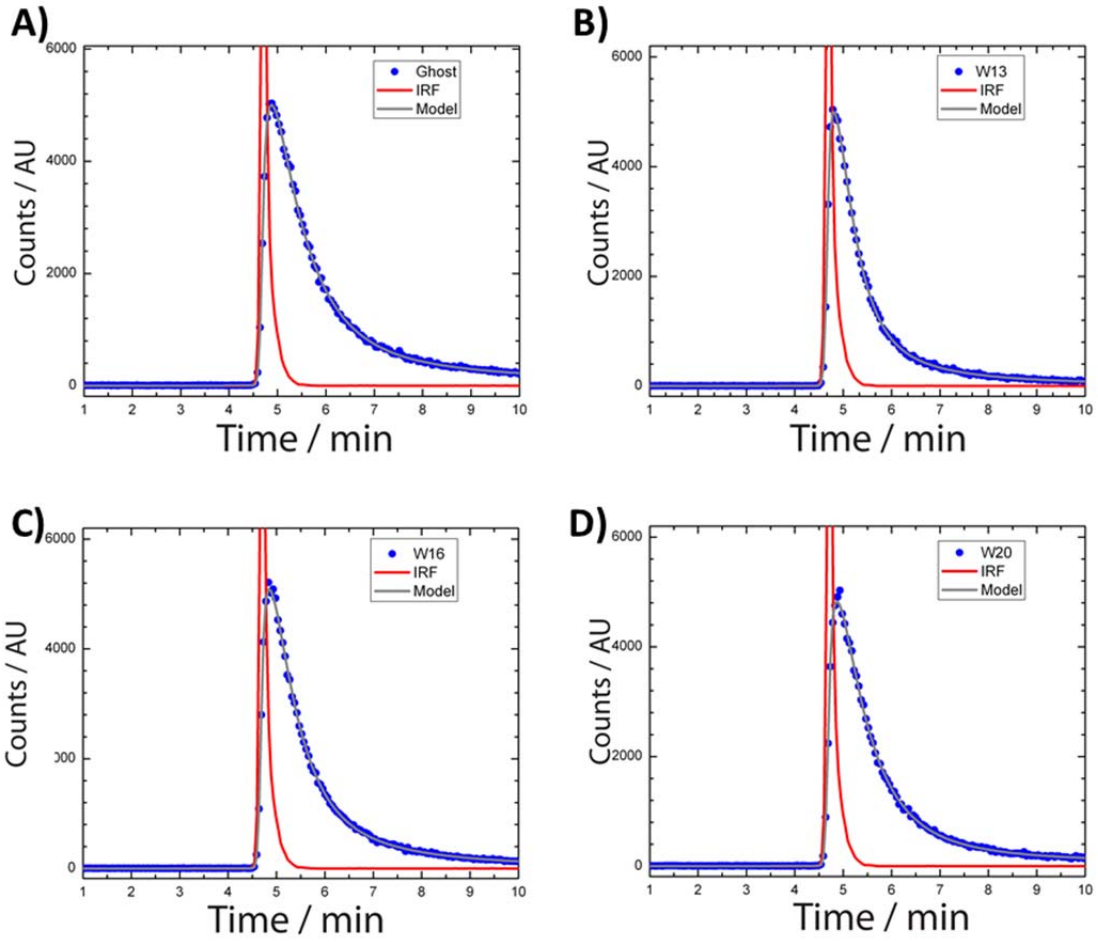

Figure S7. Time-correlated single photon counting decay curves (blue) and instrument response time functions (red) for A) the control, B) W13, C) W16, and D) W20. A 482 nm picosecond diode laser (PicoQuant GMbH) was used as an excitation source. Emission was recorded at 512 nm on a Becker-Hickl TCSPC board. The best fit to the data was triple exponential, and the average fluorescence lifetime calculated from the amplitude average is reported in Table 1.

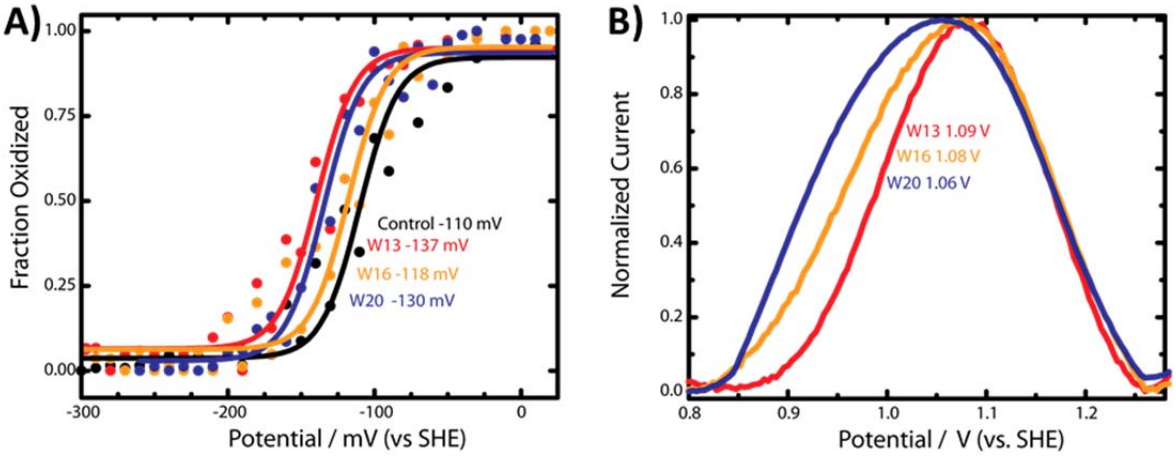

Figure S8. Redox potential of the cofactors. A) Plot of the fraction of reduced maquette calculated from the intensity of the absorption at 475 nm measured during spectro-electrochemical reduction of the flavin. The solid lines show the fit to the data from the Nernst equation for a two-electron reduction. The values of the redox potential can be found in the main text in Table 1. B) The redox potentials of TrpH/TrpH$^{\bullet+}$: W13 1.1 V, W16 1.08 V, and W20 1.06 V.

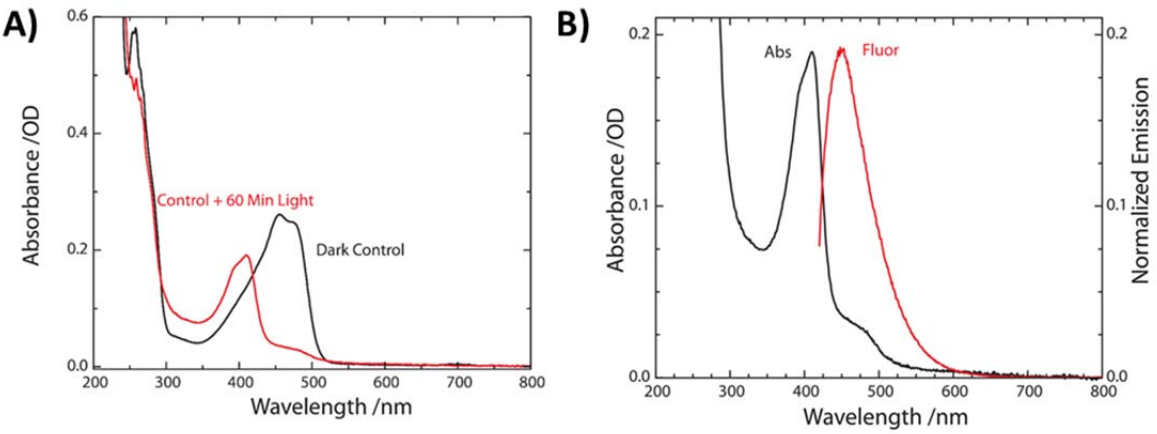

Figure S9. Characterization of the photoproduct. A) Absorption spectra of the control maquette before (black) and after (red) complete photolysis. B) Comparison of the absorption and fluorescence spectra of the photoproduct formed in A. The blue shifts of both the absorbance and fluorescence are consistent with the loss of the ribityl chain of the flavin leading to the formation of lumichrome. These features are blue-shifted relative to the literature for aqueous lumichrome, suggesting that photodegradation does not break the covalent attachment of the flavin to the maquette.

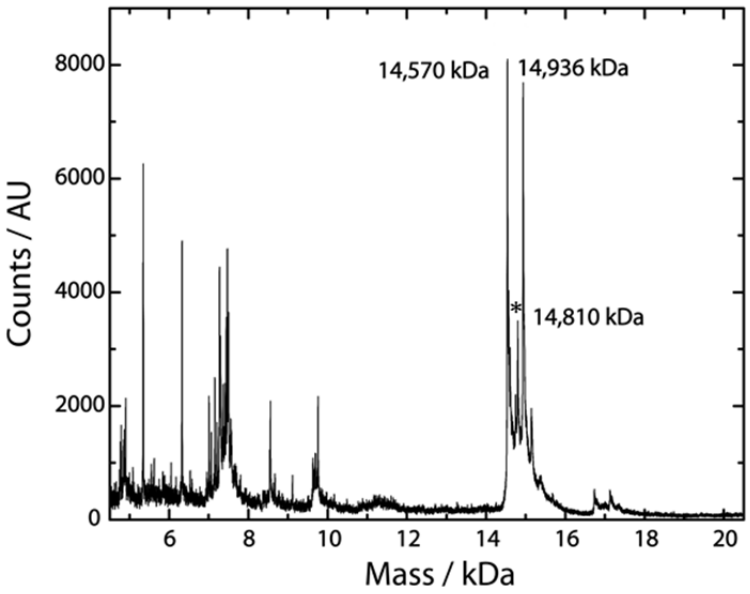

Figure S10. The MALDI-TOF mass spectrum of control maquette after photolysis. A new peak appears at 14810 *m/z* and is marked with an asterisk between the apo- and flavinated maquette signals. The mass difference after photolysis is 125 Da (± 5 Da). This is consistent with the loss of the ribityl chain and the formation of lumichrome.

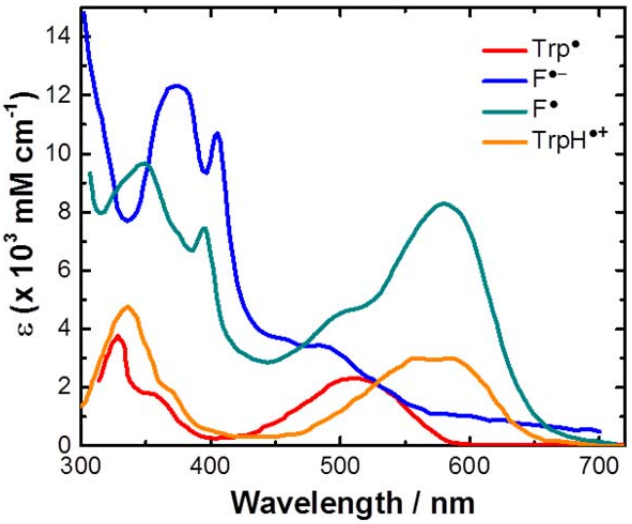

Figure S11. Reference spectra of the various protonation states of the Trp radical (red, orange),[6] and isoelectronic spectra of the flavin radicals expected after covalent attachment of flavin to the maquette: FAD radical anion bound at the 8-position to Cys (blue) from Raibekas *et al.* (2000),[7] and the neutral semiquinone radical of 8-OH-FAD (cyan) from Ghisla *et al*. (1976).[8]

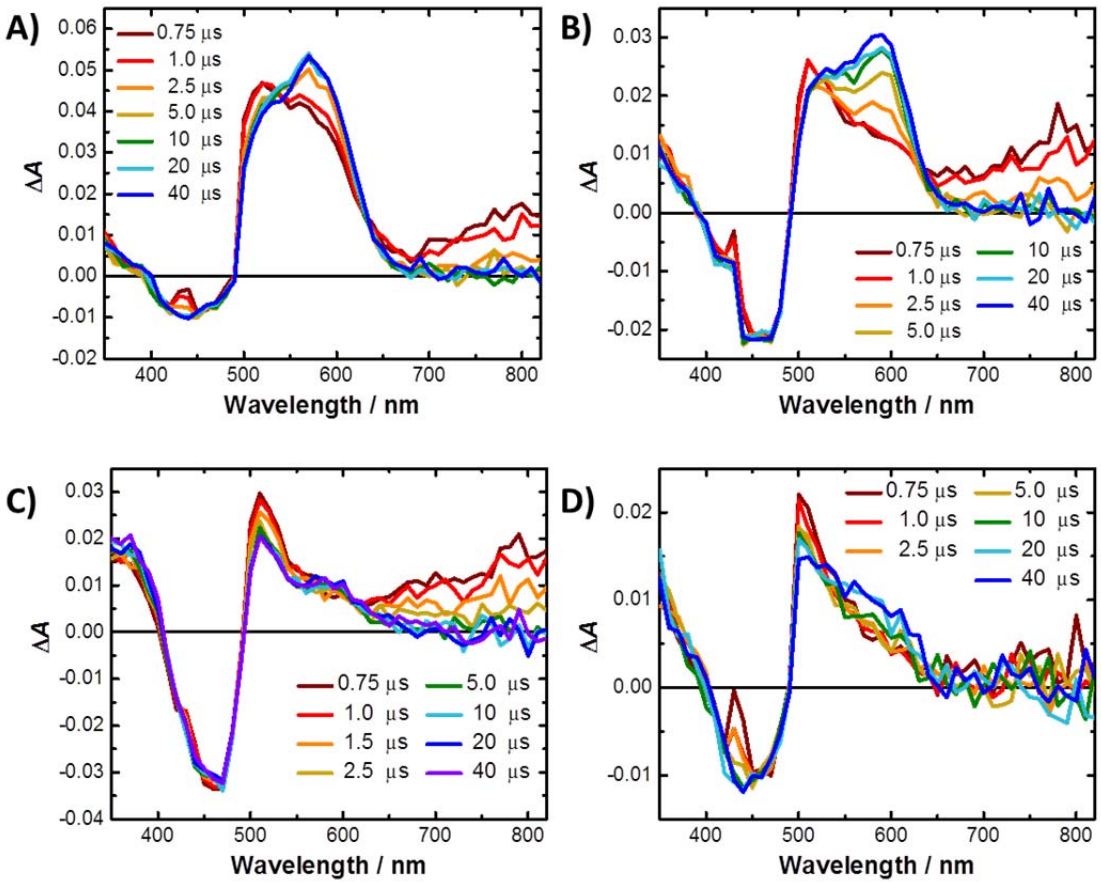

Figure S12. Transient absorption spectra of denatured control maquette (8 M urea) with 10 mM aqueous Trp. The maquette was dissolved in potassium phosphate buffer at pH 4.8 (A), 7.4 (B), and 10.2 (C). Protonation of the flavin radical is observed at low pH, as evidenced by the increase in absorbance at 580 nm. The flavin radical anion absorption dominates the spectrum at pH 10.2. Protonation of the flavin radical is less pronounced when the maquette secondary structure is intact (D, no urea in solution), but a rise in absorbance is still observed at 580 nm consistent with partial protonation to form the neutral flavin semiquinone radical.

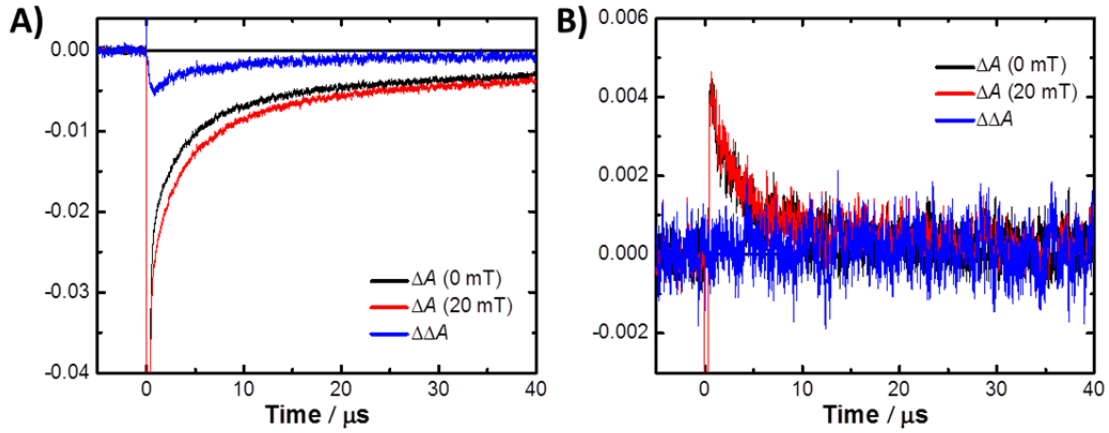

Figure S13. Kinetic traces with field-on (red) field-off (black) and the magnetic field effect (on minus off) for W16 in the region of the ground state bleach at 460 nm (A) and molecular triplet state at 800 nm (B). The absence of any subtraction signal in (B) above the noise confirms that this signal arises from triplet excited state of flavin with no magnetic field effect.

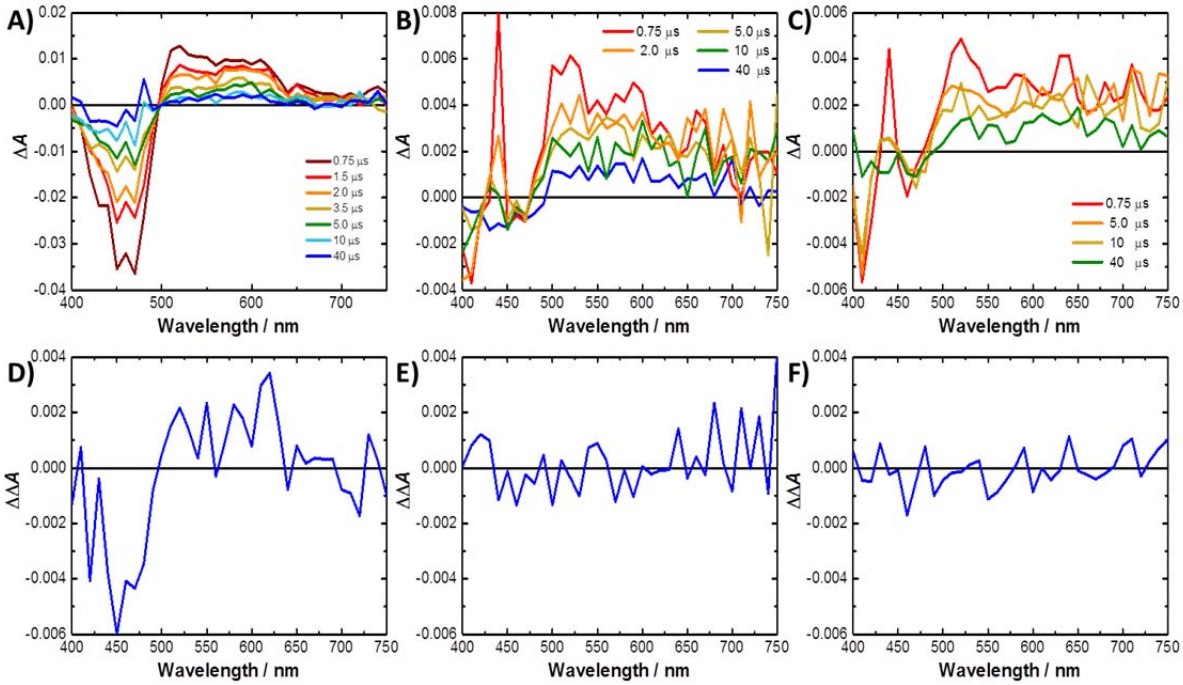

Figure S14. Transient absorption spectra of W13 (A), W20 (B), and the control maquette (C). Action spectra (D, E, F) for the above maquettes averaged over a 1 μs window beginning at 1 μs after photoexcitation. The control TA spectrum (C) shows a broad absorption feature from 500-820 nm and a weak ground state bleach. This is assigned to the molecular triplet excited state of the flavin. W13 (A) shows excited state absorption features similar to those of W16 in Figure 3A. W20 (B) shows broad, weak absorptive features from 500-820 nm, and is largely consistent with the control, although the decay at 520 nm is biexponential, which may indicate that the radical pair is formed in low quantum yield relative to W13 or W16. No MFE effect is measured for the control (F) or W20 (E). For W13, a MFE (D) of approximately 16% of the magnitude of the ESA is observed in W13 between 350-680 nm that mirrors the shape of the excited state absorption in (B).

Table S3: Kinetic analysis of transient absorption data on the single-Trp series of flavomaquettes.

Sample	λ / nm	τ_1 / µs	τ_2 / µs	Constant ($\times 10^3$)
W13	460	0.89	5.79	0.638
W13	520	1.15	6.12	0.634
W13	680-800, averaged	1.15	-	0.294
W16	460	1.71	10.83	0.636
W16	520	1.64	8.86	0.632
W16	800	1.27	-	1.074
W16	680-800, averaged	1.23	-	0.622
W20	520	21.24	1.39	0.705
W20	700	17.01	-	0.569
Control	540-620, averaged	17.24	-	1.007
Control	680-800, averaged	17.18	-	0.618

The kinetic traces were fit to a bi-exponential function with a constant offset for 460 and 520 nm. In the region of the triplet absorption, a single exponential decay was sufficient to fit the data. The value of τ_1 is attributed to decay of any triplet excited state absorption still observable on the timescale of these measurements; the value of τ_2 is assigned to the decay of the radical absorption, which is marginally faster in W13 than in W16. For W20, the lifetime of the excited triplet state is substantially longer than in W13 or W16. A shorter lifetime component which is observed in W20 at wavelengths where the radical pair is expected, but the signal intensity is not sufficient to identify the species responsible from the spectrum

References

1. Farid, T. A.; Kodali, G.; Solomon, L. A.; Lichtenstein, B. R.; Sheehan, M. M.; Fry, B. A.; Bialas, C.; Ennist, N. M.; Siedlecki, J. A.; Zhao, Z.; Stetz, M. A.; Valentine, K. G.; Anderson, J. L. R.; Wand, A. J.; Discher, B. M.; Moser, C. C.; Dutton, P. L., *Nat. Chem. Biol.* **2013,** *9*, 826-833.
2. Drössler, P.; Holzer, W.; Penzkofer, A.; Hegemann, P., *Chem. Phys.* **2002,** *282*, 429-439.
3. Moser, C. C.; Anderson, J. L. R.; Dutton, P. L., *Biochim. Biophys. Acta, Bioenerg.* **2010,** *1797*, 1573-1586.
4. Henbest, K. B.; Maeda, K.; Hore, P. J.; Joshi, M.; Bacher, A.; Bittl, R.; Weber, S.; Timmel, C. R.; Schleicher, E., *Proc. Natl. Acad. Sci. U. S. A.* **2008,** *105*, 14395-14399.
5. Ahmad, I.; Fasihullah, Q.; Vaid, F. H. M., *J. Photochem. Photobiol., B* **2005,** *78*, 229-234.
6. (a) Solar, S.; Getoff, N.; Surdhar, P. S.; Armstrong, D. A.; Singh, A., *J. Phys. Chem.* **1991,** *95*, 3639-3643; (b) Müller, P.; Bouly, J.-P.; Hitomi, K.; Balland, V.; Getzoff, E. D.; Ritz, T.; Brettel, K., *Sci. Rep.* **2014,** *4*, 5175.
7. Raibekas, A. A.; Fukui, K.; Massey, V., *Proc. Natl. Acad. Sci. U. S. A.* **2000,** *97*, 3089-3093.
8. Ghisla, S.; Mayhew, S. G., *Eur. J. Biochem.* **1976,** *63*, 373-390.